FEBS Open Bio 5 (2015) 550–556

journal homepage: www.elsevier.com/locate/febsopenbio

Histone H3 Ser57 and Thr58 phosphorylation in the brain of 5XFAD mice

Kyle W. Anderson [a,b,c], Natalia Mast [d], Irina A. Pikuleva [d], Illarion V. Turko [a,b,*]

[a] Institute for Bioscience and Biotechnology Research, Rockville, MD 20850, USA
[b] Biomolecular Measurement Division, National Institute of Standards and Technology, Gaithersburg, MD 20899, USA
[c] Department of Chemistry and Biochemistry, University of Maryland, College Park, MD 20742, USA
[d] Department of Ophthalmology and Visual Sciences, Case Western Reserve University, Cleveland, OH 44106, USA

ARTICLE INFO

Article history:
Received 10 April 2015
Revised 18 June 2015
Accepted 20 June 2015

Keywords:
Phosphorylation
Histone
5XFAD
Alzheimer's disease
Multiple reaction monitoring

ABSTRACT

Alzheimer's disease has been shown to have a global reduction in gene expression, called an epigenetic blockade, which may be regulated by histone post-translational modifications. Histone H3 has been shown to be highly regulated by phosphorylation. We, therefore, chose H3 for investigation of phosphorylation of the core sites serine-57 (S57) and threonine-58 (T58). Hemispheres of brains from a mouse model of rapid amyloid deposition (5XFAD) were used for measurement of S57 and T58 phosphorylation. Multiple reaction monitoring (MRM) was used to measure the level of phosphorylation, which was normalized to a non-modified "housekeeping" peptide of H3. S57 phosphorylation was decreased by 40%, T58 phosphorylation was decreased by 45%, and doubly phosphorylated S57pT58p was decreased by 30% in 5XFAD brain in comparison to C57BL/6J age- and sex-matched wild type controls. Amyloid-β (Aβ) and amyloid precursor protein were also measured to confirm that 5XFAD mice produced high levels of Aβ. Decreased phosphorylation of these sites in close proximity to DNA may lead to stabilization of DNA–histone interactions and a condensed chromatin state, consistent with the epigenetic blockade associated with AD. Our findings of H3 sites S57 and T58 exhibiting lower levels of phosphorylation in 5XFAD model compared to wild type control implicate these sites in the epigenetic blockade in neurodegeneration pathology.

1. Introduction

Alzheimer's disease (AD) is the most common neurodegenerative disorder and is the sixth leading cause of death in the U.S. [1]. The cause of AD is still not well understood and there is no disease-modifying treatment to delay onset or slow progression [2,3]. Epigenetics of AD is a growing field that has gained interest due to the repression of gene transcription, an epigenetic blockade, that is consistently observed in AD [4,5]. Among these changes associated with gene repression are post-translational modifications (PTMs) of histones, which can alter histone–DNA and inter-nucleosome interaction and, in turn, chromatin structure [6]. PTMs are largely found on the N-terminal domains, commonly referred to as tail regions, that extend from the histone core complex. Little information exists on PTMs in the core region of histones.

One common PTM on histones is phosphorylation of serine (Sp) and threonine (Tp) residues, which has been linked to activation and repression of genes based on site of modification and condition of cells [7–9]. Serine phosphoacceptor sites are found on the tail regions of all core histones [10]. Phosphorylation of S10 on histone H3 (H3S10p) has been extensively studied for its roles in condensation of chromatin during mitosis [8,9] and to a lesser extent in neurodegenerative disorders, such as AD [11]. While many types of PTMs on histone tails have been associated with disease, little information exists on PTMs in the core region of histones. It is suggested that phosphorylation of H3 may be particularly meaningful compared to other core histones [7,12,13]. Specifically in the core region of H3, there are several potential threonine and serine phosphorylation sites, but exploration of their significance has been minimal. H3T45p is directly correlated with apoptosis [14], H3T80p is increased in mitosis [15], and H3T118p destabilizes the nucleosome [16]. However, little is known about H3S57 and H3T58 phosphorylation roles in normal biological functions and there is no information to date describing changes in these phosphorylation sites in AD brain. H3S57p has been detected in mammalian cells and may have implications in response to DNA damage based on studies in yeast [17]. H3T58p has not been

Abbreviations: Aβ, amyloid-β; APP, amyloid precursor protein; MRM, multiple reaction monitoring; PTM, post-translational modification; S57, serine-57; T58, threonine-58

* Corresponding author at: Institute for Bioscience and Biotechnology Research, 9600 Gudelsky Drive, Rockville, MD 20850, USA. Tel.: +1 240 314 6257.
E-mail address: iturko@umd.edu (I.V. Turko).

http://dx.doi.org/10.1016/j.fob.2015.06.009
2211-5463/Published by Elsevier B.V. on behalf of the Federation of European Biochemical Societies.

previously characterized. Additionally, we investigated *in silico* potential phosphorylation sites on the surface of the nucleosome which could be easily accessible to kinases and phosphatases and found that S57 and T58 are located on the surface. Specifically, these adjacent residues occur in an accessible turn of a helix-turn-helix motif of H3 in close proximity to DNA, which suggests these sites may engage in regulatory phosphorylation and supports investigation into these sites in brain and AD pathology.

AD is characterized by deposition of amyloid-β (Aβ) plaques and neurofibrillary tangles of tau protein as well as dementia. The Aβ peptide is contained in the amyloid precursor protein (APP), a large integral membrane protein concentrated in neurons. In AD, APP undergoes processing by membrane-anchored proteases, called secretases, producing the amyloidogenic isoform Aβ42. The γ-secretase complex, consisting of protein nicastrin, APH1, PEN2, and presenilin 1 (PS1) or PS2, executes the C-terminal cleavage of Aβ, releasing the intracellular domain (ICD) of APP into the cytoplasm. In addition to releasing the ICD of APP, γ-secretase can also cleave Notch and other proteins. Released ICDs may act as signaling molecules, for example the Notch ICD can activate nuclear signaling pathways [18]. Released Aβ may form neurotoxic oligomers or aggregate into senile plaques in the extracellular environment [19]. To mimic the amyloid pathology found in humans with AD, transgenic mice with genetic mutations that cause rapid amyloid deposition have been created as models of AD pathology [20]. One of these models, called 5XFAD mice, overexpress two human proteins with five mutations of familial AD: PS1 with M146L and L286V and APP695 with Swedish (K670N, M671L), Florida (I176V), and London (V717I) mutations. In addition to vast overproduction of Aβ42, these 5XFAD mice also display cognitive impairment consistent with dementia [20]. We used the 5XFAD mouse model of rapid amyloid deposition as our subject for investigation of H3 phosphorylation at S57 and T58 sites.

Our study shows that phosphorylation of both S57 and T58 on histone H3 is lower in 5XFAD models of amyloid deposition in comparison to wild type controls. Since changes in PTMs of histones are established to influence genetic expression, our measurements of specific histone H3 residues S57 and T58 may provide insight into the epigenetic blockade phenomenon in the pathology of neurodegeneration.

2. Material and methods

The DC Protein Assay kit was purchased from Bio-Rad Laboratories (Hercules, CA). RapiGest SF surfactant was from Waters (Milford, MA), Trypsin (T0303, Type IX-S from porcine pancreas) and all other chemicals were purchased from Sigma–Aldrich (St. Louis, MO).

2.1. Mice

All animal-handling and experimentation performed was approved by the Institutional Animal Care and Use Committee at Case Western Reserve University. 5XFAD [20] mice were maintained by crossing 5XFAD hemizygous males on B6SJL background (The Jackson Laboratory) with B6SJL females (The Jackson Laboratory, stock 100012). Only F1 males homozygous with respect to the transgene were used. Wild type C57BL/6J mice (The Jackson Laboratory, stock 000664), a common laboratory strain that do not develop amyloid plaques and the progenitor strain used to make transgenic 5XFAD, were used as control. Mice were housed in the Animal Resource Center at Case Western Reserve University and maintained in a standard 12 h light/12 h dark cycle environment. Water and food were provided ab libitum. 5XFAD male mice ($n = 3$) and C57BL/6J age- and sex-matched wild type controls ($n = 3$) were sacrificed at 3 months of age to assess the differences.

2.2. Whole mouse brain processing

Hemispheres of brains were harvested and flash-frozen in liquid nitrogen for storage at −80 °C. Left hemispheres of the brain were finely minced with a scalpel blade and homogenized in 25 mmol/L NH_4HCO_3 by sonication at 30 W using five, 10 s continuous cycles (Sonicator 3000, Misonix Inc., Farmingdale, NY). Total protein concentration of the homogenate was measured using a DC protein assay kit in the presence of 1% (mass fraction) sodium dodecyl sulfate (SDS) with bovine serum albumin as the standard. Homogenates were aliquoted and stored at −80 °C. Samples of 3 mg total protein were supplemented with 12 pmol APP QconCAT standard [21] and treated with 20 mmol/L dithiothreitol (DTT) and 1% (mass fraction) SDS. After 1 h incubation at room temperature to reduce cysteines, 55 mmol/L iodoacetamide was added and incubated an additional 1 h to alkylate cysteines. Chloroform/methanol precipitation was used to isolate proteins. Protein pellets were then sonicated in 1 mL 25 mmol/L NH_4HCO_3/0.1% (mass fraction) RapiGest SF surfactant and treated with trypsin at 25:1 protein:trypsin mass ratio overnight at 37 °C. After trypsinolysis, 0.5% (volume fraction) trifluoroacetic acid (TFA) was added and incubated at 37 °C for 1 h to cleave acid-labile RapiGest SF surfactant, which was subsequently removed by centrifugation at 179,000*g* for 30 min at 4 °C. Supernatants were dried in an Eppendorf AG Vacufuge (Hamburg, Germany), yielding final peptides for analysis.

2.3. LC–MS/MS analysis

Dried peptides were reconstituted in 3% acetonitrile, 97% water, and 0.1% formic acid (volume fraction). Separation was performed on an Agilent Zorbax Eclipse Plus C18 RRHD column (2.1 mm × 50 mm, 1.8 μm particle) and multiple reaction monitoring (MRM) analysis was performed on an Agilent 6490 iFunnel Triple Quadrupole LC/MS system (Santa Clara, CA). Peptides were eluted at a flow rate of 200 μL/min using the following gradient of solvent B in solvent A: 3% B for 3 min, 3–30% B in 32 min, 30–50% B in 5 min, and 50–3% B in 3 min. Solvent A was water containing 0.1% (volume fraction) formic acid and solvent B was acetonitrile containing 0.1% formic acid. The acquisition method used the following parameters in positive mode: fragmentor 380 V, collision energy 20 V, dwell time 100 ms, cell accelerator 4 V, electron multiplier 500 V, and capillary voltage 3500 V. MRM transitions for 2+ charge precursor ions and 1+ charge product ions were predicted using PinPoint software (Thermo Fisher Scientific, Waltham, MA).

2.4. Data analysis for APP and Aβ

Quantification of total APP and Aβ in mouse brain samples, using MRM with QconCAT as an internal standard [21], was performed to confirm that the 5XFAD model of amyloid pathogenesis produced significant Aβ in comparison to the control. A QconCAT is a recombinant protein containing concatenated peptides used for multiplexed quantification of proteins [22]. The QconCAT standard used contained peptides for both APP and Aβ [21] and was supplemented into homogenates prior to processing to increase precision and accuracy of measurements. Based on sequence specificity and measured intensity, a single peptide, LVFFAEDVGSNK, was selected from Aβ and two peptides, VESLEQEAANER and AVIQHFQEK, were selected to measure total APP. APP is large transmembrane protein that undergoes processing to release the fragment Aβ. Therefore,

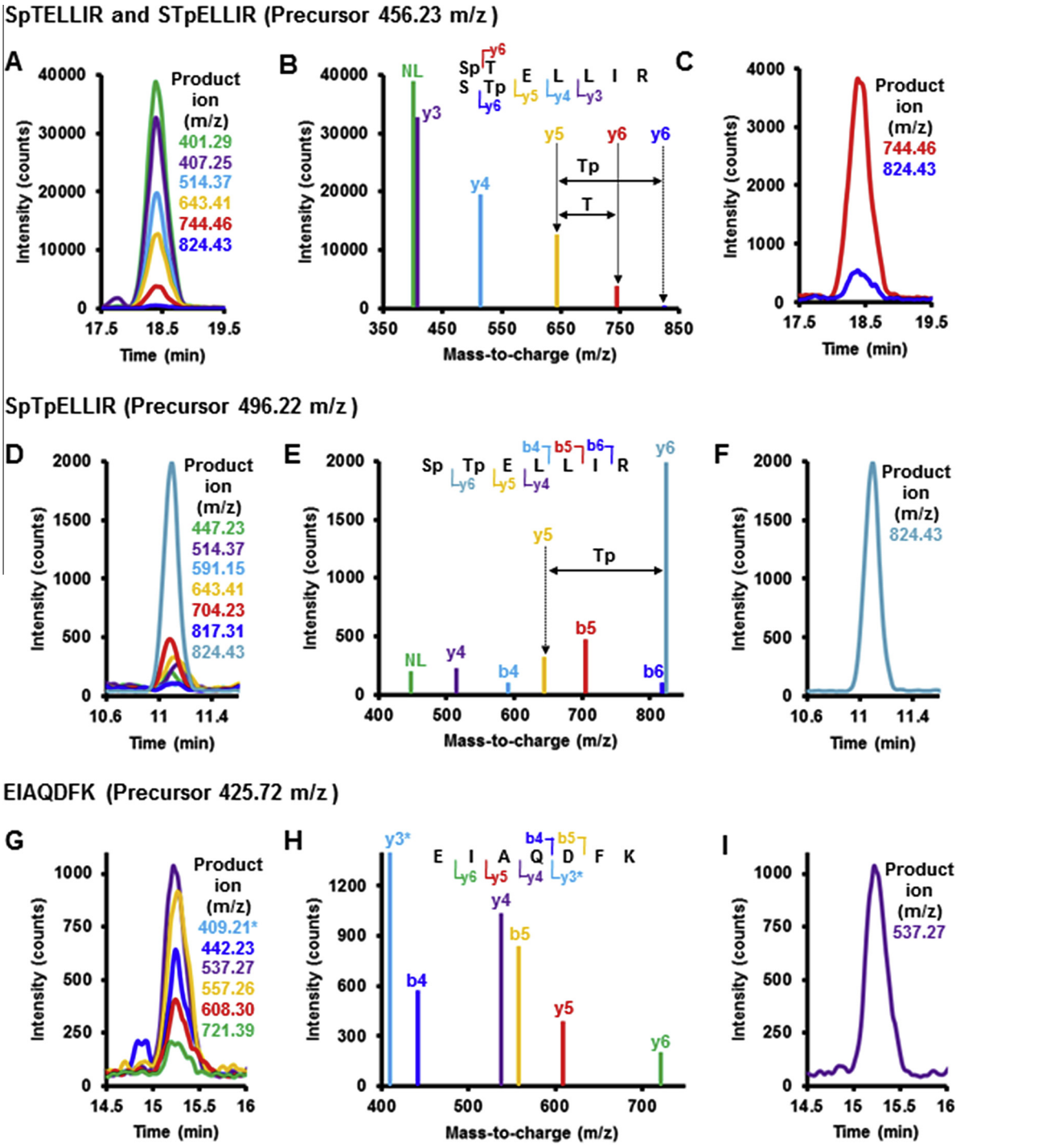

Fig. 1. Peptide identification by MRM and selection of transitions for quantification. (A, D and F) Numerous transitions were monitored to determine retention time and confirm identity of each peptide. (B, E and H) Spectra of ions used to confirm identity and site of phosphorylation. (C, F and I) A single transition was selected from each peptide for quantification. *Transition 425.72 → 409.21 had high signal intensity and was removed from chromatogram (G) and reduced in spectrum (H) to better illustrate other monitored transitions.

the Aβ amino acid sequence is part of the APP protein. Measurements for Aβ are inclusive of the Aβ fragment and unprocessed APP, which still contains Aβ. These peptides were included in a stable isotope labeled QconCAT standard, as previously described [21], which was supplemented into samples. Quantification of APP and Aβ was performed by calculating the ratio of peak areas for unlabeled biological peptides to labeled standard peptides using MassHunter software (Agilent) multiplying by the ratio of known picomoles of standard to milligrams of total protein. Protein concentrations are presented as pmol/mg and represent the mean ± standard deviation (SD) of peptide transitions associated with each protein. Statistical significance of mean differences was calculated using Student's two-tailed *t*-test and was considered significant if $p \leqslant 0.05$. Transitions used for quantification of APP and Aβ are presented in Supplementary Table S1.

2.5. Data analysis for phosphorylation

All selected MRM transitions were used to confirm the identity of each peptide for each LC–MS analysis and a representative transition for each peptide was chosen for quantification. Quantitative transitions were stable in replicate injections and produced signal reasonable for comparison to those of other peptides. Additionally, the ratio of quantitative transitions to respective transitions for each precursor was consistent across biological samples, indicating quantitative transitions were not biased. A list of all transitions for identification and quantification are available in Supplementary Table S2. Peak areas of quantitative transitions were calculated using MassHunter software from Agilent. Peak areas of phosphorylated peptides were normalized to peak area of calibrant peptide, EIAQDFK, found in the core of H3. EIAQDFK was initially screened in both control and 5XFAD mice for any PTMs and none were detected, allowing for its use as a calibrant peptide. Triplicate biological replicates, each with triplicate analytical replicates, produced $n = 9$ normalized ratios, which were averaged together and presented as mean ± standard deviation. Statistical significance of mean differences was calculated using Student's two-tailed t-test. An example of calculations from raw integrated peak areas to normalized and averaged values is presented in Supplementary Table S3.

3. Results and discussion

3.1. Preparation of brain samples for measurement

To minimize unwanted loss of phosphorylation, SDS was added to tissue homogenates at the very first step of sample processing to arrest enzymatic activity. Early addition of SDS also efficiently denatures proteins [23,24] and evenly exposes Cys residues in all samples to subsequent reduction and alkylation. The main H3 variants, H3.1, H3.2, and H3.3, all contain a cysteine at position 110 that is known to undergo disulfide bonding to form an H3 dimer. H3.1, in addition, contains a cysteine at position 96 that participates in disulfide bonding [25,26]. A challenge to processing brain tissue for MS analysis is its high lipid content, which can degrade chromatography performance and contribute to ion suppression. The whole brain is approximately 80% lipid by dry mass [27] and, therefore, necessitates removal of lipids. Chloroform/methanol precipitation of the protein efficiently removed lipids, SDS, salts, and by-products alkylation to yield a pure protein pellet. These two major steps, (i) early addition of SDS followed by reduction/alkylation of Cys residues and (ii) chloroform/methanol precipitation to increase protein purity, ensure sample quality compatible with LC–MS/MS analyses, while minimizing processing to maintain endogenous phosphorylation. Additionally, all samples were processed in parallel to ensure that no artificial loss of phosphorylation would create a bias between samples groups and that observed differences between groups were purely of biological origin.

3.2. Selection of transitions for MRM

The main histone H3 variants, H3.1, H3.2, and H3.3, have very close homology, which is evidenced by their sequence alignment (Supplementary Fig. S1). Initially, all selected transitions for peptides containing only S57p, only T58p, or both S57p and T58p were used to identify and confirm retention times of peptides in each MS chromatogram (Fig.1). With the specificity of MRM and consensus of six or more transitions for each peptide, peptide identification was performed with certainty. The most abundant, unique transition for each peptide was then used for quantification using integrated peak area. By selecting the most abundant transition for quantification, peak area could be more reproducibly and accurately measured. Transitions used for identification and quantification can be found in Supplementary Table S2. Our measurements using this method of relative quantification enable comparison of the level of change in S57 and T58 phosphorylation in the AD model 5XFAD to control.

3.3. APP and Aβ in 5XFAD brain

Mice with rapid amyloid deposition (5XFAD) [20] were compared to age- and sex-matched wild type C57BL/6J mice. 5XFAD provide an appropriate model for AD-related amyloid pathogenesis for the exploration of amyloid-associated changes [28]. Aβ was 460 ± 70 pmol/mg total protein in 5XFAD mouse brain, a 177-fold greater concentration than the 2.6 ± 0.2 pmol/mg in control (Fig. 2). APP was 54 ± 3 pmol/mg in 5XFAD, 13-fold greater than the 4.1 ± 0.5 pmol/mg in control (Fig. 2). The significant increase in APP and Aβ indicates the presence of amyloid pathology in the 5XFAD mouse brain. Since the amino acid sequence for Aβ is present in both free Aβ and unprocessed APP (Fig. 2A), it is of interest to compare the level of Aβ to APP to verify that Aβ concentration increases were not largely attributed to unprocessed APP. In

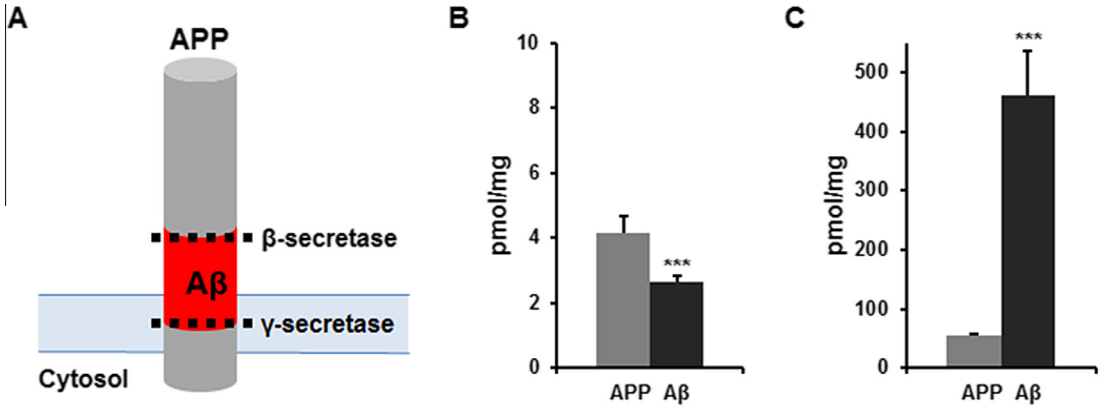

Fig. 2. Quantification of APP and Aβ in 5XFAD and control. (A) Amyloid precursor protein, APP, (gray) is a large transmembrane protein that contains the amino acid sequence for Aβ (red). Aβ is released as a fragment peptide during processing of APP by β- and γ-secretases. Therefore, measurements for Aβ include the peptide present in unprocessed APP and free Aβ. Total APP peptides AVIQHFQEK and VESLEQEAANER and Aβ peptide LVFFAEDVGSNK were measured in whole hemisphere homogenates from (B) wild type mice ($n = 3$) and (C) 5XFAD mice ($n = 3$). Measurements represent mean ± standard deviation of biological replicates ($n = 3$) using three transitions for AVIQHFQEK, four transitions for VESLEQEAANER, and four transitions for LVFFAEDVGSNK for absolute quantification using QconCAT as internal standard. $^{***}p < 0.001$.

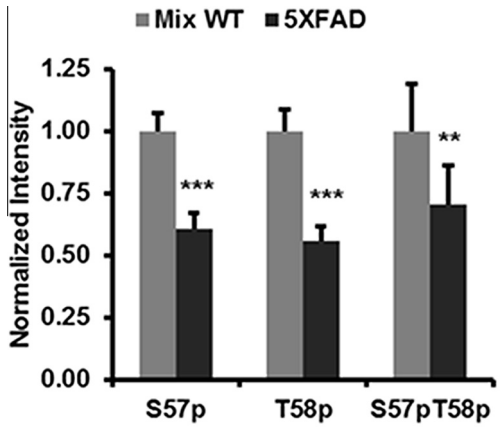

Fig. 3. Effect of 5XFAD model on S57 and T58 phosphorylation. Phosphorylation was measured in whole hemisphere homogenates from mixed wild type mice ($n = 3$) and 5XFAD mice ($n = 3$). Measurements represent mean ± standard deviation of biological and analytical replicates ($n = 9$) normalized to respective phosphorylation site in mixed wild type control. $^{**}p < 0.01$; $^{***}p < 0.001$.

control mice, the 4.1 ± 0.5 pmol/mg of APP was similarly low in concentration to 2.6 ± 0.2 pmol/mg of Aβ. However, in 5XFAD, the 460 ± 70 pmol/mg of Aβ is nearly 9-fold greater than the 54 ± 3 pmol/mg of APP, indicating a large increase in Aβ not attributed to unprocessed APP. Additionally, our inclusion of SDS and RapiGest denaturants facilitated the unfolding and solubilization of Aβ for proteolysis, therefore our measurements represent the total amount of solubilized Aβ. Our measurements confirm that 5XFAD mice produce significantly more Aβ than control mice in the brain (Fig. 2). Our findings validated the use of 5XFAD as a model of rapid amyloid pathogenesis for subsequent quantification of phosphorylation of S57 and T58 residues.

3.4. S57 and T58 phosphorylation of 5XFAD brain

A representative transition for each peptide was chosen for quantification of phosphorylation. Quantitative transitions were stable in replicate injections and produced good signals for comparison. Moreover, the ratio of quantitative transitions to other transitions from the same precursor was consistent across biological samples, indicating quantitative transitions were not biased. Peak areas of transitions from phosphorylated peptides were normalized to peak area of transition from calibrant peptide, EIAQDFK, found in the core of H3 (Supplementary Table S3). Data was obtained from three mice per sample group and each mouse was analyzed in triplicate ($n = 9$ total measurements) to properly assess statistically significant differences between sample groups.

As compared to C57BL/6J mice, 5XFAD showed a 40% lower level of S57p, 45% lower level of T58p, and a 30% lower level of simultaneously phosphorylated S57p and T58p (Fig. 3). The decrease in phosphorylation of S57 and T58 might have an impact on nucleosome stability. S57 is less than 1.1 nm from DNA (Fig. 4A) and T58 is less than 0.9 nm from DNA (Fig. 4B) in the crystal structure of the human nucleosome, PDB ID: 2CV5 [29]. These distances

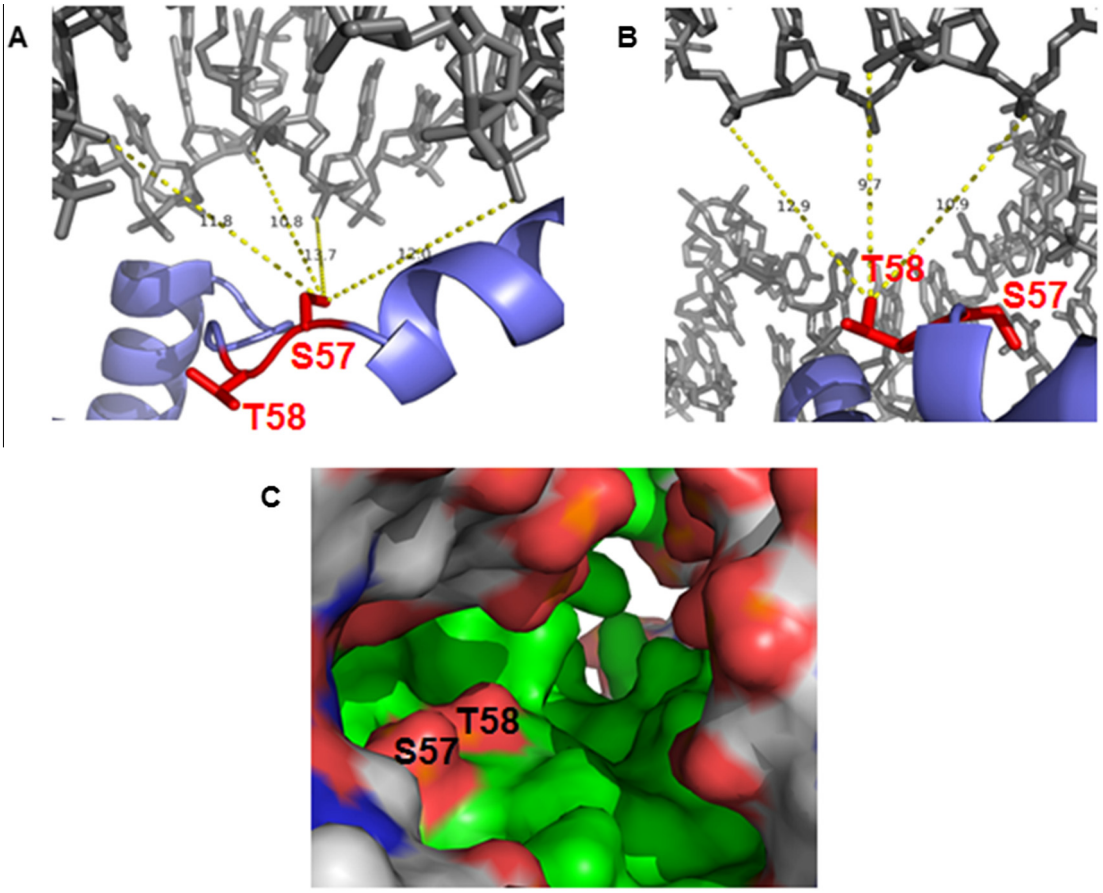

Fig. 4. Proximity of H3 S57 and T58 to DNA. (A) S57 is less than 1.1 nm from DNA and (B) T58 is less than 0.9 nm from DNA. DNA is shown in gray, H3 in blue, and S57 and T58 sites in red. Distance measurements were performed in PyMOL Molecular Graphics System Version 1.7.2 using the crystal structure of the human nucleosome (PDB ID: 2CV5) [29]. (C) Surface view of phosphorylated S57 and T58 on histone core (green) in close proximity to the interface of the positively charged phosphate backbone (red) of DNA (gray). All modeling was performed in PyMOL and insertion of phosphate groups was performed using a PyMOL plugin called PyTMs [30].

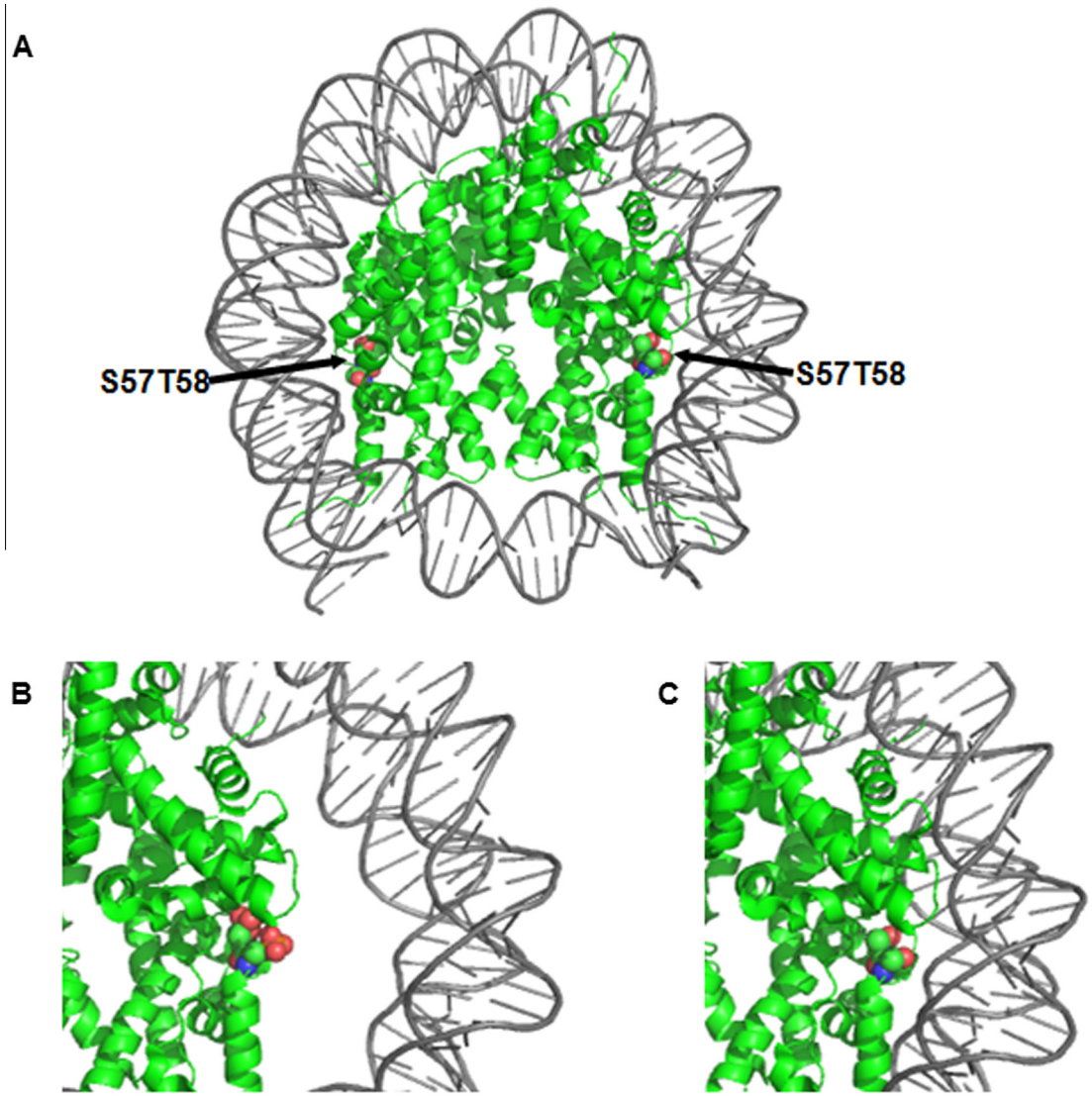

Fig. 5. Location of H3 residues S57 and T58 within nucleosome. (A) Core histones (green), with flexible histone tails truncated in structure, is shown wrapped in DNA (gray). The S57T58 regions (spheres with oxygen in red and nitrogen in blue) are in the turn of a helix-turn-helix motif that brings the residues in close proximity to DNA and are easily accessible to kinases and phosphatases. (B) Phosphorylated S57 and T58 create a repulsive charge–charge interaction with negatively charged DNA, weakening the affinity of the nucleosome. (C) Dephosphorylation of S57 and T58 greatly reduces negative charge on the histone interface, strengthening the affinity of the DNA–histone interaction. Modeling was performed using PyMOL Molecular Graphics System Version 1.7.2 and the crystal structure of the human nucleosome (PDB: 2CV5) [29]. Insertion of phosphate groups was performed using the PyTMs plugin [30].

were measured with PyMOL Molecular Graphics System (Version 1.7.2, Schrödinger, LLC). Phosphorylation of S57 and T58 causes a significant increase in negative charge in close proximity to the negatively charged phosphate backbone of DNA (Fig. 4C). Furthermore, both residues are on the histone surface and are positioned in a turn of a helix-turn-helix motif of the H3 polypeptide chain, highlighting the ease of access by modifying enzymes (Fig. 5A). Introduction of phosphoryl groups, about 0.25 nm in size, in close proximity to the negatively charged backbone of DNA can weaken DNA–histone interactions [16] (Fig. 5B). Conversely, dephosphorylation, as observed in 5XFAD (Fig. 5C), can strengthen nucleosome stability and lead to condensed chromatin with reduced gene expression [16], consistent with AD pathology [4,5]. Our measurements reveal dephosphorylation of S57 and T58 in 5XFAD, which may illustrate specific epigenetic changes that occur in AD.

In summary, we demonstrate that MRM assay can provide relative quantification of phosphorylation of histone H3 residues S57 and T58 in lipid-rich, whole mouse brain homogenates. We show that levels of S57p, T58p, and doubly phosphorylated S57 and T58 decrease in 5XFAD mice. This suggests these histone PTMs play an epigenetic role in AD pathology and may stabilize nucleosomes, causing decreased gene transcription. Our measurements contribute to the overall understanding of AD pathology and may provide clinical targets for pharmaceutical intervention.

Acknowledgments

The authors declare no competing financial interest. Certain commercial materials, instruments, and equipment are identified in this manuscript in order to specify the experimental procedure as completely as possible. In no case does such identification imply a recommendation or endorsement by the National Institute of Standards and Technology nor does it imply that the materials, instruments, or equipment identified are necessarily the best available for the purpose.

This work was supported in part by the U.S. Public Health Service Grant GM62882 (to I.A.P.) and EY11373 (P30 Core grant) to Case Western Reserve University. I.A.P. is a recipient of the Jules and Doris Stein Professorship from the Research to Prevent Blindness. APP standard was kindly provided by Dr. Junjun Chen at Institute of Bioscience and Biotechnology Research in Rockville, MD.

K.W.A., I.V.T., and I.A.P. conceived and designed the project, K.W.A. acquired and analyzed the data, and K.W.A. and I.V.T. wrote the manuscript. N.M. raised and harvested brains from mice. All authors revised the manuscript for important intellectual content and gave final approval of the version to be published.

Appendix A. Supplementary data

Supplementary data associated with this article can be found, in the online version, at http://dx.doi.org/10.1016/j.fob.2015.06.009.

References

[1] The Alzheimer's Association (2012) 2012 Alzheimer's disease facts and figures. Alzheimers Dement. J. Alzheimers Assoc. 8, 131–168.
[2] Holtzman, D.M., Morris, J.C. and Goate, A.M. (2011) Alzheimer's disease: the challenge of the second century. Sci. Transl. Med. 3, 77.
[3] Lindsley, C.W. (2012) Alzheimer's disease: development of disease-modifying treatments is the challenge for our generation. ACS Chem. Neurosci. 3, 804–805.
[4] Gräff, J., Rei, D., Guan, J.-S., Wang, W.-Y., Seo, J., Hennig, K.M., Nieland, T.J.F., Fass, D.M., Kao, P.F., Kahn, M., Su, S.C., Samiei, A., Joseph, N., Haggarty, S.J., Delalle, I. and Tsai, L.-H. (2012) An epigenetic blockade of cognitive functions in the neurodegenerating brain. Nature 483, 222–226.
[5] Sananbenesi, F. and Fischer, A. (2009) The epigenetic bottleneck of neurodegenerative and psychiatric diseases. Biol. Chem. 390, 1145–1153.
[6] Izzo, A. and Schneider, R. (2010) Chatting histone modifications in mammals. Briefings Funct. Genomics 9, 429–443.
[7] Clayton, A.L., Rose, S., Barratt, M.J. and Mahadevan, L.C. (2000) Phosphoacetylation of histone H3 on c-fos- and c-jun-associated nucleosomes upon gene activation. EMBO J. 19, 3714–3726.
[8] Hendzel, M.J., Wei, Y., Mancini, M.A., Van Hooser, A., Ranalli, T., Brinkley, B.R., Bazett-Jones, D.P. and Allis, C.D. (1997) Mitosis-specific phosphorylation of histone H3 initiates primarily within pericentromeric heterochromatin during G2 and spreads in an ordered fashion coincident with mitotic chromosome condensation. Chromosoma 106, 348–360.
[9] Wei, Y., Mizzen, C.A., Cook, R.G., Gorovsky, M.A. and Allis, C.D. (1998) Phosphorylation of histone H3 at serine 10 is correlated with chromosome condensation during mitosis and meiosis in Tetrahymena. Proc. Natl. Acad. Sci. USA 95, 7480–7484.
[10] Loury, R. and Sassone-Corsi, P. (2003) Histone phosphorylation: how to proceed. Methods San Diego Calif 31, 40–48.
[11] Ogawa, O., Zhu, X., Lee, H.-G., Raina, A., Obrenovich, M.E., Bowser, R., Ghanbari, H.A., Castellani, R.J., Perry, G. and Smith, M.A. (2003) Ectopic localization of phosphorylated histone H3 in Alzheimer's disease: a mitotic catastrophe? Acta Neuropathol. (Berl.) 105, 524–528.
[12] Cheung, P., Allis, C.D. and Sassone-Corsi, P. (2000) Signaling to chromatin through histone modifications. Cell 103, 263–271.
[13] Jenuwein, T. (2001) Translating the histone code. Science 293, 1074–1080.
[14] Hurd, P.J., Bannister, A.J., Halls, K., Dawson, M.A., Vermeulen, M., Olsen, J.V., Ismail, H., Somers, J., Mann, M., Owen-Hughes, T., Gout, I. and Kouzarides, T. (2009) Phosphorylation of histone H3 Thr-45 is linked to apoptosis. J. Biol. Chem. 284, 16575–16583.
[15] Hammond, S.L., Byrum, S.D., Namjoshi, S., Graves, H.K., Dennehey, B.K., Tackett, A.J. and Tyler, J.K. (2014) Mitotic phosphorylation of histone H3 threonine 80. Cell Cycle (Georget. Tex) 13, 440–452.
[16] North, J.A., Javaid, S., Ferdinand, M.B., Chatterjee, N., Picking, J.W., Shoffner, M., Nakkula, R.J., Bartholomew, B., Ottesen, J.J., Fishel, R. and Poirier, M.G. (2011) Phosphorylation of histone H3(T118) alters nucleosome dynamics and remodeling. Nucleic Acids Res. 39, 6465–6474.
[17] Zielinska, D.F., Gnad, F., Jedrusik-Bode, M., Wiśniewski, J.R. and Mann, M. (2009) Caenorhabditis elegans has a phosphoproteome atypical for metazoans that is enriched in developmental and sex determination proteins. J. Proteome Res. 8, 4039–4049.
[18] Mumm, J.S. and Kopan, R. (2000) Notch signaling: from the outside in. Dev. Biol. 228, 151–165.
[19] Haass, C. and Selkoe, D.J. (2007) Soluble protein oligomers in neurodegeneration: lessons from the Alzheimer's amyloid beta-peptide. Nat. Rev. Mol. Cell Biol. 8, 101–112.
[20] Oakley, H., Cole, S.L., Logan, S., Maus, E., Shao, P., Craft, J., Guillozet-Bongaarts, A., Ohno, M., Disterhoft, J., Van Eldik, L., Berry, R. and Vassar, R. (2006) Intraneuronal beta-amyloid aggregates, neurodegeneration, and neuron loss in transgenic mice with five familial Alzheimer's disease mutations: potential factors in amyloid plaque formation. J. Neurosci. Off. J. Soc. Neurosci. 26, 10129–10140.
[21] Chen, J., Wang, M. and Turko, I.V. (2013) Quantification of amyloid precursor protein isoforms using quantification concatamer internal standard. Anal. Chem. 85, 303–307.
[22] Cheung, C.S.F., Anderson, K.W., Wang, M. and Turko, I.V. (2015) Natural flanking sequences for peptides included in a quantification concatamer internal standard. Anal. Chem. 87, 1097–1102.
[23] Liao, T.-H. (1975) Reversible inactivation of pancreatic deoxyribonuclease a by sodium dodecyl sulfate. J. Biol. Chem. 250, 3831–3836.
[24] Womack, M.D., Kendall, D.A. and MacDonald, R.C. (1983) Detergent effects on enzyme activity and solubilization of lipid bilayer membranes. Biochim. Biophys. Acta 733, 210–215.
[25] Hake, S.B. and Allis, C.D. (2006) Histone H3 variants and their potential role in indexing mammalian genomes: the "H3 barcode hypothesis". Proc. Natl. Acad. Sci. USA 103, 6428–6435.
[26] Camerini-Otero, R.D. and Felsenfeld, G. (1977) Histone H3 disulfide dimers and nucleosome structure. Proc. Natl. Acad. Sci. USA 74, 5519–5523.
[27] O'Brien, J.S. and Sampson, E.L. (1965) Lipid composition of the normal human brain: gray matter, white matter, and myelin. J. Lipid Res. 6, 537–544.
[28] Hong, I., Kang, T., Yoo, Y., Park, R., Lee, J., Lee, S., Kim, J., Song, B., Kim, S.-Y., Moon, M., Yun, K.N., Kim, J.Y., Mook-Jung, I., Park, Y.M. and Choi, S. (2013) Quantitative proteomic analysis of the hippocampus in the 5XFAD mouse model at early stages of Alzheimer's disease pathology. J. Alzheimers Dis. 36, 321–334.
[29] Tsunaka, Y., Kajimura, N., Tate, S. and Morikawa, K. (2005) Alteration of the nucleosomal DNA path in the crystal structure of a human nucleosome core particle. Nucleic Acids Res. 33, 3424–3434.
[30] Warnecke, A., Sandalova, T., Achour, A. and Harris, R.A. (2014) PyTMs: a useful PyMOL plugin for modeling common post-translational modifications. BMC Bioinformatics 15, 370.